

We are IntechOpen, the world's leading publisher of Open Access books Built by scientists, for scientists

6,900

Open access books available

186,000

International authors and editors

200M

Downloads

Our authors are among the

154

Countries delivered to

TOP 1%

most cited scientists

12.2%

Contributors from top 500 universities



WEB OF SCIENCE™

Selection of our books indexed in the Book Citation Index
in Web of Science™ Core Collection (BKCI)

Interested in publishing with us?
Contact book.department@intechopen.com

Numbers displayed above are based on latest data collected.
For more information visit www.intechopen.com



High-Speed and High-Resolution Photon Counting for Near-Range Lidar

Tatsuo Shiina

Additional information is available at the end of the chapter

<http://dx.doi.org/10.5772/intechopen.74350>

Abstract

The near-range lidars for hard target and atmosphere detection should follow to the quick motion/activity of the measurement target. The transmitting optical power will be lowered for safety in the human activity space. And the lidar should increase the pulse repetition frequency to get the enough signal-to-noise ratio. The high-speed, high-resolution and high-repetition photon counting is desired for the near-range lidar. It is not a single photon counting at a certain delay time, but a multi-channel scaler with a deep memory for a series of delay times, that is, ranging data acquisition for lidar application. In this chapter, the mini-lidar for near-range observation is discussed. The targets are dust, gas, and atmosphere (aerosols). The activity monitoring of the atmosphere within a few hundred meters is the purpose of this mini-lidar. To follow and visualize the rapid motion of the target, high-speed and high-resolution photon counters (multi-channel scalers) were developed. The observation range can be easily adjustable depending on the lidar setup. The system can visualize the rapid motion of target with the high-resolution of 0.15 m (BIN width of 1 ns) and the minimum summation time of 0.2 s.

Keywords: lidar, dust, atmosphere, high-speed, scaler

1. Introduction

Nowadays, Near-range lidar; Light Detection And Ranging, is of a particular interest in viewpoint of safety management [1–8]. The word “lidar,” however, is used for both of hard target detection and atmospheric/gas detection. The former does not need the high sensitivity in general, but when the target moves quickly, and when the detecting target is a transparent material, the detector sensitivity should be high. The latter needs the high-sensitivity especially for low concentration gas and low altitude atmosphere, which moves rapidly depending on a

structure, terrain, and the altitude. The photon counting is one of the choices in such high-sensitive lidar. Our attention is on such a rapid activity measurements of the atmosphere, dust and a certain gas.

The near-range lidars for hard target and atmosphere detection should follow to the quick motion/activity of the target material. The transmitting optical power will be lowered for safety in the human activity space. And the lidar should increase the pulse repetition frequency to get the enough signal-to-noise ratio. The high-speed, high-resolution and high-repetition photon counting is desired for near-range lidar. It is not a single photon counting at a certain delay time, but a multi-channel scaler with a deep memory for a series of delay times, that is, ranging data acquisition for lidar application.

The LED-based mini-lidar for near-range observation is considered in this Chapter. The optical pulsed power of 1nJ is emitted at the pulse width of 10 ns. The activity monitoring of the atmosphere within a few hundred meters is the purpose of this mini-lidar. To follow and visualize the rapid motion of the target, high-speed and high-resolution photon counters (multichannel scalers) were developed. The LED mini-lidar emits the pulsed beam at the pulse repetition frequency of >500 kHz, while the developed photon counter counts the echo signals at the summation time of only 0.2 s at a minimum. The observation range can be easily adjustable depending on the lidar setup. The system can visualize the rapid motion of target with the high-resolution of 0.15 m (BIN width of 1 ns) at the interval of 0.2 s.

At first, the needs of near-range lidar with some fields are explained. Afterwards, The lidar setup will be discussed in the viewpoint of near-range detection. The architecture of the high-speed photon counting is mentioned in the content. The design of the signal processing is considered to optimize the lidar echo detection. Some concrete applications are mentioned as well. At the end, the next step of the high-speed photon counting is finally discussed.

2. Lidar principle and photon counting

2.1. Lidar setup and equations

“Lidar,” “LiDAR” or “Laser Radar” come from the word of Radar: Radio Detecting and Ranging. Lidar consists of transmitter part, receiver part and signal processing part. **Figure 1** shows the typical setup of lidar system. The pulsed laser beam was collimated and fired into the atmosphere with almost parallel to the receiver’s optical axis. The optical receiver is adjusted its field of view (FOV) to detect the lidar echo from the target with an adequate signal-to-noise ratio. A traditional lidar has individual optics (biaxial optics) for a laser transmitter and a receiver, and the system has a blind area, which the transmitting beam cannot enter within a receiver’s FOV, especially in near range. The blind area also causes in the case of coaxial optics that the beam is transmitted within a receiver’s aperture. As the receiver’s FOV is wider, or the beam divergence is wider, the blind area will be shortened, while the background light enters a lot into the receiver. As a result, the signal-to-noise ratio of the lidar echo will be lower. The lidar echo is detected by high sensitive detectors such as photomultiplier

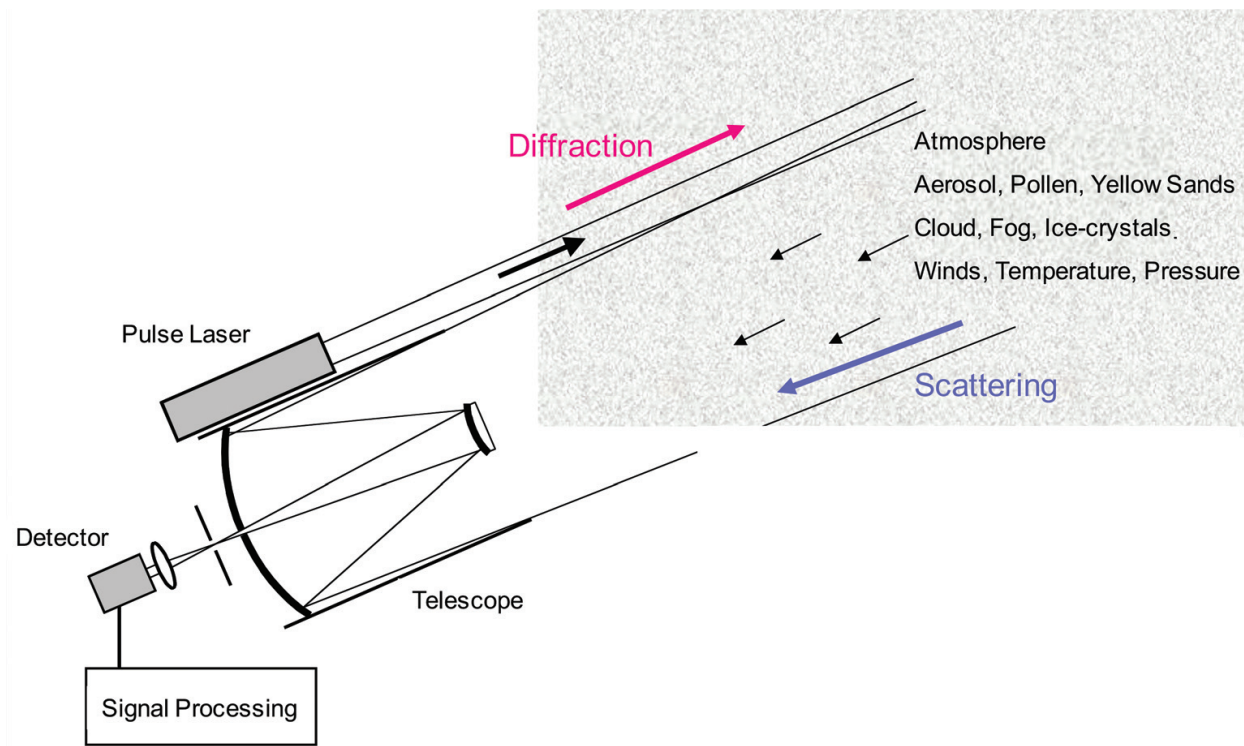


Figure 1. Fundamental setup of lidar system and target samples.

and Avalanche Photo Diode (APD), and stored in PC via a digitizer. When the lidar echo becomes weak and hard to detect an analog signal, photon counting method is selectable. When the collimated beam penetrates the atmosphere, it is attenuated by suspended particles in the atmosphere. As the atmospheric extinction coefficient is represented as α , the transmittance T obeys to the Beer-Lambert's law as follows

$$T(L) = \exp \left[- \int_0^L \alpha(x) dx \right] \quad (1)$$

where L is the propagation distance of the beam. When the beam hits the particles, the scattered lights go back to the same path. The echo, however, is also attenuated by the particles in the return path. Furthermore, the scattered echo spreads in all direction, and its intensity decreases in inversely proportional to the square of the distance because the scattering energy is spread in spherical. The lidar echo power depends on the atmospheric characteristics and also depends on the optical characteristics of the lidar apparatus such as the aperture of the optical receiver, the pulse width of the transmitting beam, the optical efficiency of the lidar system [9–10]. The concrete lidar echo power $P(L)$ is estimated by the lidar equation,

$$P(L) = P_0 K Y(L) A_r \frac{c\tau}{2} \beta(L) T(L)^2 / L^2 \quad (2)$$

where P_0 is the transmitted power [W], K is the system optical efficiency, A_r is the aperture of the optical receiver [m^2], c is the speed of light [m/s], τ is the pulse width of the beam [s], $\beta(L)$ is

the backscattering cross section of the target [m^{-1}], $Y(L)$ is the geometrical form factor, which is the overlap function between the transmitting beam and the receiver's field of view. It is determined by the telescope specification, the beam divergence, and the size of the field stop aperture; FSA. The geometrical form factor decides the initial receiving characteristics in near range. When you will observe the near-range target, its lidar echo can be corrected by this factor. After the blind area, there is the intermediate distance where the beam partially crosses into the field of view. Here the lidar echo power rises up till the whole of the beam enters in the field of view.

To estimate the signal-to-noise ratio of the lidar echo; SNR, is effective to evaluate the practical lidar echo under the several noises. You should consider the influences of the background light and the noise factor of the detector. The signal-to-noise ratio is written as

$$SNR(L) = \frac{\sqrt{M}\sqrt{\eta\Delta t/h\nu P(L)}}{\sqrt{\mu}\sqrt{P(L) + P_b + P_d}} \quad (3)$$

where η is the detector's quantum efficiency, Δt is the sampling interval [s], μ is the detector's noise factor, which is typically equal to 2–3 for APD and 1 for PMT, h is Planck's constant [J s], ν is the light frequency [Hz], P_b is the background light power [W], P_d is the equivalent dark current power [W], M is the number of signal summations. That is, the long-term summation will increase the SNR, but its effect does not increase linearly. The numerator of the Eq. (3) improves SNR by the detector's sensitivity and the summation. The denominator weakens SNR by the noises of the atmosphere and the lidar system.

2.2. Analog mode and digital mode

The lidar signal is captured by the photo detector. It is an optical intensity and changes to the electric current. The current is, in general, the flow of many electrons. In the current flow, each electron is not distinguished. This is an analog mode. The lidar echo was come from suspended particles in the air and cause the electric current via a photodetector. The echo intensity as the current is inversely proportional to the square of the distance as shown in lidar Eq. (2). On contrary, the current becomes weak, and the individual electrons behave as discrete flows of pulse responses. In this situation, the lidar echo becomes stochastic scattering process at each distance. The photon signals indicate that the echo intensity is represented by not its signal height, but by its density in a certain time period. It is an photon counting mode (digital mode). **Figure 2** shows such behavior difference on analog mode and photon counting mode of the lidar echo.

2.3. Principle of photon counting

Discrete photon signals are captured by high speed photon detector. Nano-seconds' rise time can follow these discrete signals. The Photo Multiplier Tube (PMT) and Avalanche Photo Diode (APD) are used as photon counting device. In the case of PMT, the device, which the dark current is enough low, is selected as a photon counting device [11]. In the case of APD, the

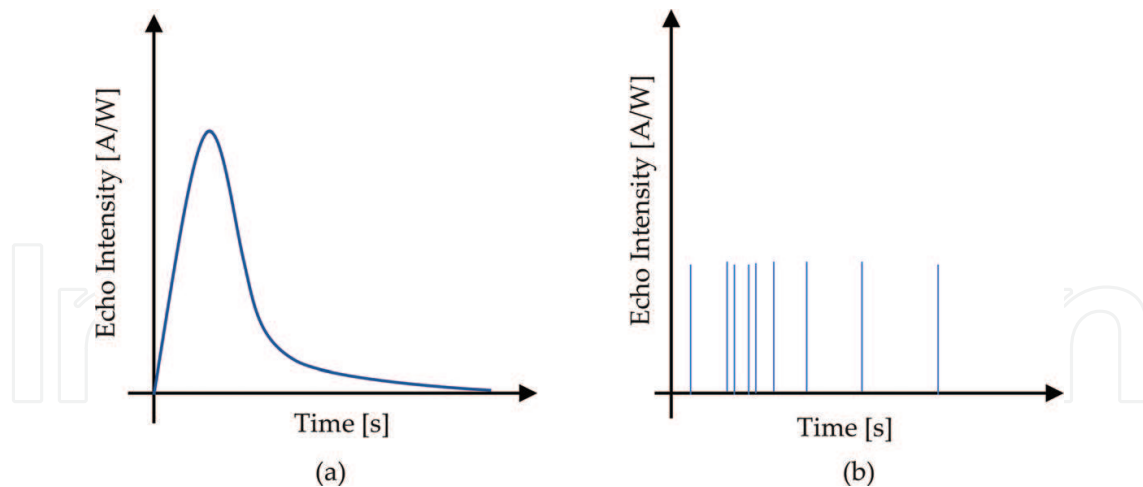


Figure 2. Analog signal (a) and discrete photon signals (b).

high voltage just below its breakdown voltage is implied. APD's photon counting is often called as Geiger mode [12].

Photon counting provides the echo counted numbers within a certain period. Usual photon counting will change the delay time one after another to capture a whole feature of the waveform. It is good for the repeatable echo signal. The sudden change and the intermittent echoes sometimes appear in the atmospheric lidar echo, especially in near range and low altitude echoes. In such a case, the delay time shift should be enough rapid and the echo counts at each delay time will be put in individual counters, which is called as BIN. Series BINs capture the echo counts due to the delay time. Such a device calls "scaler." BIN width indicates the time resolution, which is equivalent with the range resolution. The number of BINs represents the maximum detectable range. The repetition rate or repetition frequency is also the property of the photon counting. It decides the detectable phenomena of the target activity. The balance of the BIN width, its number, and repetition frequency is important for the photon counting device.

In the past, the memory and delay shifter and sequencer was assembled to make rearise the photon counter. Nowadays, however, fruitful functions installed FPGA boards are selectable. Therefore, high-speed and high-precision photon counter can be designed more easily and systematically.

3. Near-range Lidar

3.1. Time scale and spatial scale

The compact lidar is suitable to the near-range observation of less than a few 100 m, while the traditional large lidar is good at the long-range observation from a few kilometers to a 100 km. The compact lidar, however, is not a down-size one of the large lidar. **Table 1** shows the spatial

Phenomena	Spatial scale	Time scale
HP/LP	1000 km	10 h
Typhoon	100 km	3 h
Convection	50 km	2 h
Thunder clouds	10 km	1 h
Cumulus	2 km	10 min
Down burst	600 m	7 min
Tornado	200 m	5 min
Boundary layer	60 m	10 s

Table 1. Spatial and time scales of atmosphere.

and time scales in atmospheric phenomena. The large phenomena such as HP/LP have a large spatial and time scales, while the small phenomena like tornado takes small spatial and time scales. That is, the small phenomena become small structure and quick motion. To detect and visualize such small phenomena, the compact lidar should follow with the quick motion with high resolution. Furthermore, near-range detection is often a sensing in human living space. In that meaning, the transmitting optical power should keep eye-safety. It causes the limit of transmitting power and the selection of optical wavelength.

3.2. Transmitter and receiver requirements

Dust activity in low altitude is rapid, and the lidar should be high-speed and high-resolution detection. The BIN width of the photon counter decides spatial resolution. Pulse width of the transmitting beam is also shortened until the time that at least the detector can response. In the near-range observation, the transmitting beam will be thrown in horizontal direction. the transmitting power should be controlled in the view point of eye-safety. To make a margin to the signal-to-noise ratio under the restriction of the transmitting power, the pulse repetition frequency will be increased.

The lidar is not efficient in the near-range detection because of blind area. To shorten the blind area, the easy way is to give a small tilt to the transmitting beam against the receiver's optical axis. The receiver's field of view (FOV) is narrow of the order of a few milli-radians, and the optical alignment becomes severe. The transmitting beam has its power to spare, its divergence will be wider than the receiver's FOV. The lidar optics is free from misalignment and the system becomes robust. **Figure 3** shows the overlap efficiency of the lidar optics. The main graph (right) indicates the transmitting/receiving ratio under the transmitting beam divergence of 10 mrad. The sub-graph (left) shows the overlap function in the lidar Eq. (2) and its shift to the transmitting/receiving ratio. In the case that the receiver's FOV is 5 and 3 mrad, the transmitting/receiving ratio keeps 30 and 10%, respectively. In other words, when the transmitting beam power has a margin of 3–10 times compared with its usual operation, one can utilize this advantage.

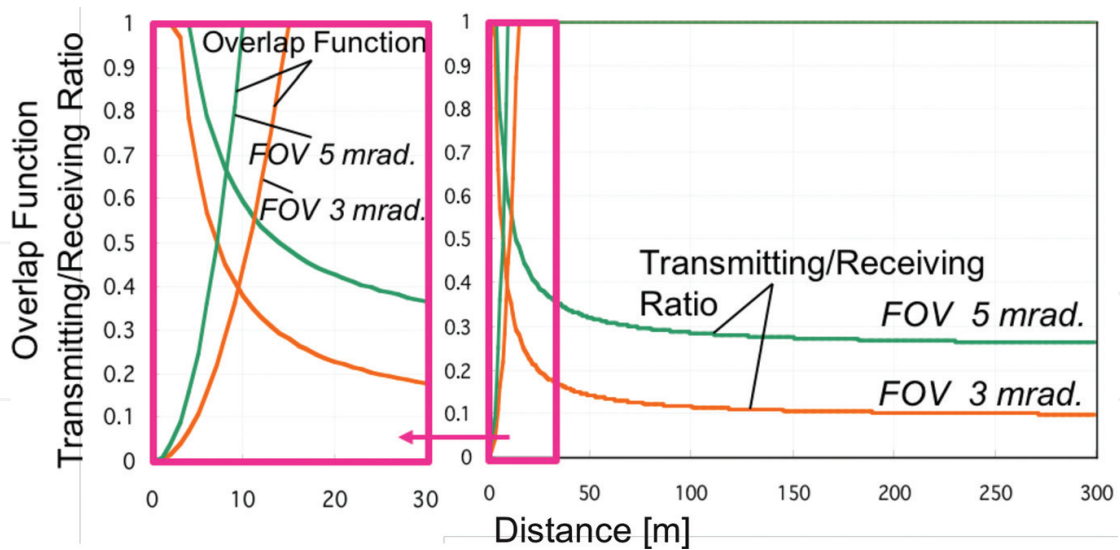


Figure 3. Overlap efficiency of lidar optics.

3.3. Near-range lidar setup

The near-range lidar is better to be compact or mini-size, light weight, and low electric power consumption. The traditional lidar does not have these features because the higher atmosphere has a slow activity, which depends on the altitude in general. The low altitude atmosphere change more quickly due to the ground surface, structure, and weather conditions. Dust flow and a certain gas behavior also follow to the atmosphere activity.

Figure 4 shows one of examples of the LED based mini-lidar optics [13–15]. Its specification is summarized in Table 2. The Lamp-type LED of 3 mm ϕ is installed for lidar light source. Its transmitting pulse power is 200 mW ($\approx 2\text{nJ}/10\text{ns}$). Average power is less than 1 mW. The wavelength is 392 nm and its spectral band width is 10 nm. Beam divergence is controlled to 5 mrad with a Fresnel lens of 50 mm ϕ . The receiver is a Cassegrain-type telescope of the



Figure 4. LED-based mini-lidar.

Transmitter	Light source	Lamp-type UV-LED(3mm ϕ)
	Wavelength	Center 392 nm, Width 10 nm
	Pulse width	10 ns
	Repetition frequency	380 kHz
	Pulse power	200 mW
	Beam divergence	5 mrad
Receiver	Beam size	50 mm ϕ
	Telescope type	Cassegrain
	Aperture	102 mm ϕ
	Field of view	3 mrad
	Interference filter	Center 394 nm, Width 10 nm
	Detector	PMT (photon counting purpose)

Table 2. Specification of LED-based mini-lidar.

aperture of 102 mm ϕ . The interference filter of the center wavelength 394 nm and its band width 10 nm is installed, too. The PMT for photon counting mode is selected for high sensitive detector. The LED-based mini-lidar is compact (150 mm(W) \times 150 mm(H) \times 300 mm(D)), light weight (<3 kg), and low electric power consumption (\sim 2 W). The observation range is more than 100 m for atmosphere observation. The electrical power is fixed 12 V, and it can be operated with not only AC adapter but also with small DC battery.

The pulse power and its repetition frequency are 200 mW and 380 kHz, respectively. The pulse repetition frequency is increased to compensate the low transmitting power. It is hard for the traditional photon counting device to follow to this high repetition frequency. The high-speed and high-resolution photon counter was originally developed.

4. High-speed and high-resolution photon counting

4.1. Architecture

Now several kinds of FPGA (Field-programmable gate array) boards are available. FPGA is one of complex programmable logic device (CPLD). These boards have various kinds of functions such as high-speed signal processing, long memory, plural interfaces and so on. For the lidar application, not only high-speed signal processing but long memory is important. The fundamental architecture is shown in **Figure 5**. At first, lidar signal from the detector is connected into a comparator. It will judge that the signal height exceeds a threshold or not. FPGA device prepares the plural counters (BINs) and de-multiplexer, which shifts the connecting counters due to the delay time. Each discrete echo pulses are entered into the counters due to the delay time. The delay time is generated by the system clock. The trigger

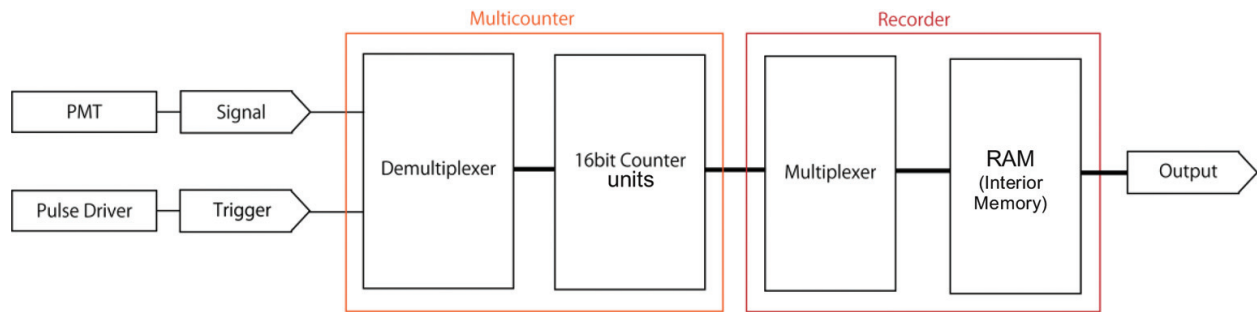


Figure 5. Fundamental architecture of photon counter.

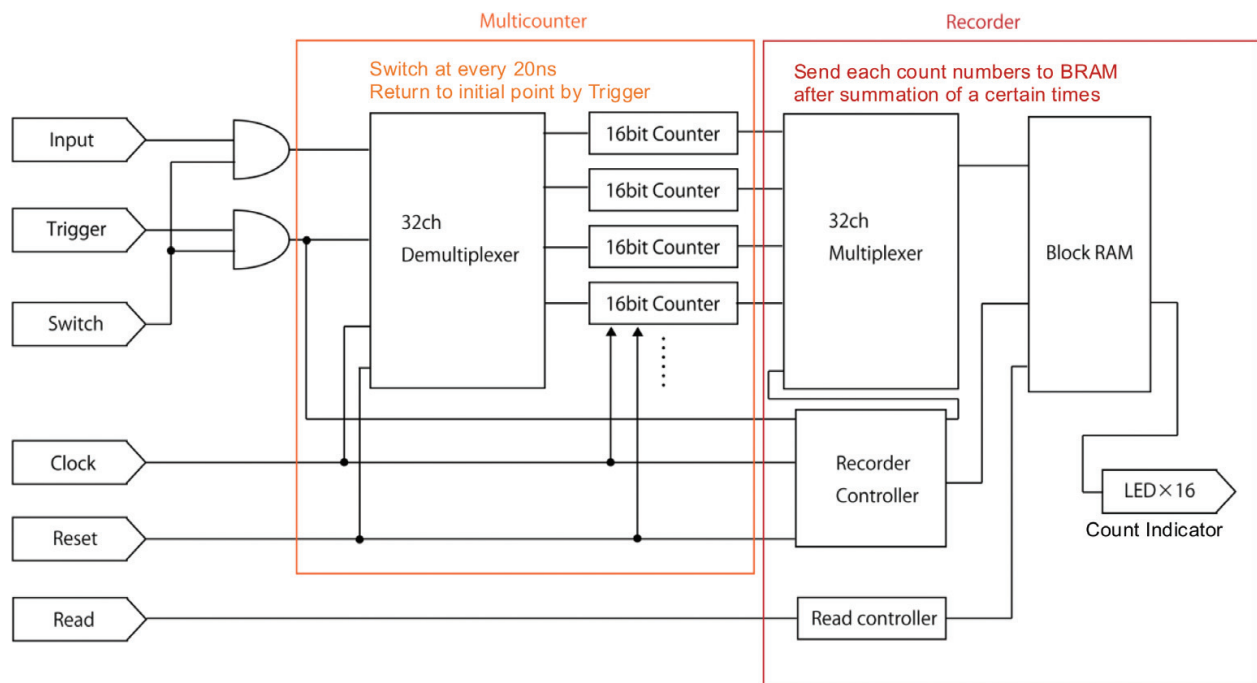


Figure 6. Concrete sketch of signal process on FPGA device.

signal is synchronous to the transmitting pulse beam. This trigger signal links to the repetition frequency of the FPGA process to return the first counter, that is, the nearest distance. After the defined number of times repeats, each counter sends its counted numbers to a memory via a multiplexer. Speed of system clock, FPGA process and memory capacity should have a balance to process the signal on time.

The programming of FPGA device is conducted by Verilog HDL. At first, we fabricated a prototype with a FPGA board (Digilent Basys 2). It is a FPGA trainer board. The FPGA device is Spartan-3E, Xilinx. System clock is 300 MHz. The block RAM is 72 kb. The concrete program design is shown in **Figure 6**. For lidar setup, the 50MHz operation was selected. It is equivalent to BIN width of 20 ns and the range resolution of 3 m. The BIN number is 25, which defines the maximum range of 75 m. The repetition frequency is 500 kHz. The result was successful to detect the sea wave motion with the summation time of 0.2 s.

4.2. FPGA photon counting board

After the trial development, the concrete photon counting board was developed with the help of a company. The schematic diagram and its specification are shown in **Figure 7** and **Table 3**, respectively. The developed photon counting board has 4-channel inputs. They are convenient for multi-channel observation such as orthogonal polarization measurement, certain gas Raman scattering observation, and multi-wavelength detections. The board can be synchronized to the pulse beam oscillation by trigger in port. On contrary, the board can generate the trigger signal to fire the pulse beam.

This photon counting board is commercialized by Trimatiz Co., Ltd., [16]. The FPGA device is Spartan 6, Xilinx. The system clock is 500 MHz. The PC interface to communicate the board setup and to transfer lidar data is PCI express. The board size is 111 × 168 mm. It is the size of expansion board of half size in desktop PC. Power consumption is 7 W, that is, <2 W for each channel. This photon counting board is able to connect parallel till three boards. Synchronous operation is possible up to 12 channels. The board feature is shown in **Figure 8**.

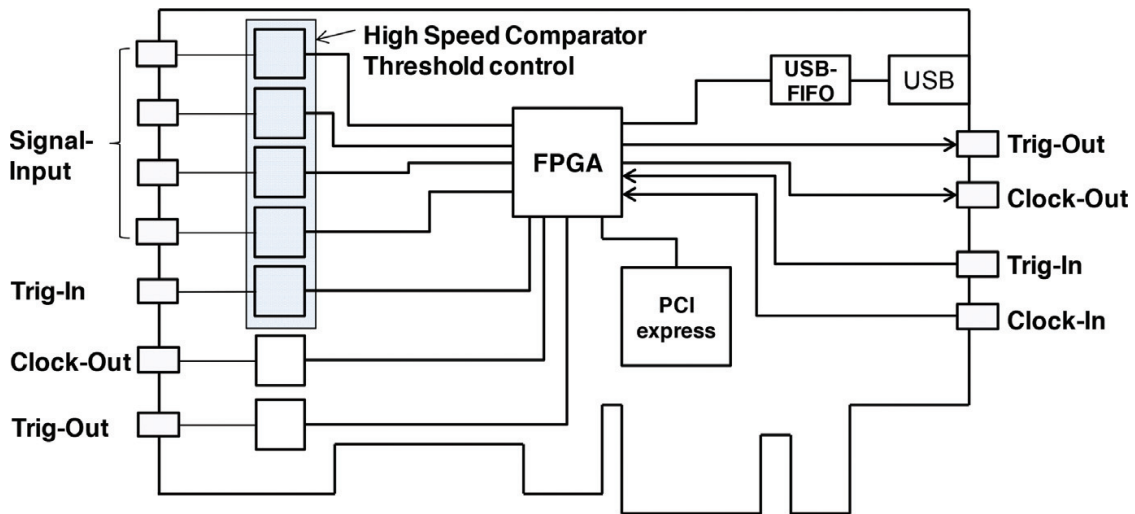


Figure 7. FPGA photon counter board.

FPGA device	Spartan 6
System clock	550 MHz
BIN width	5 ns–10.486 ms [5 ns × 2 ⁿ (n = 0–21)]
Number of BINs	32,767
Maximum counts	32,767
Input channel	1–4 (expands to 8–12)
Repetition frequency	>300 kHz
Interface	PCI express

Table 3. Specification of FPGA photon counting board.



Figure 8. FPGA photon counting board (Photon tracker, Trimatiz Co., Ltd.).

The specialized software is bundled to control the FPGA board. The BIN width and number, repetition frequency, threshold and trigger levels, can be adjustable. The highest resolution defined by BIN width is 5 ns, which is equal to the range resolution of 0.75 m. the minimum summation time up to the data transformation to PC is 0.2s.

4.3. Improvement

After the development of the first FPGA photon counting board, minor arrangement was accomplished. The PC interface change to the USB port for convenience via an adapter. As a next generation, the clock signal was integrated by a division program. As a result, the minimum special resolution is accomplished 1 ns, that is, 0.15 m. The repetition frequency is kept the high-speed of 500kHz. Minimum summation time is 0.2s with the enough BIN numbers. In this minimum summation time, the obtained data is stored in a memory within a certain repetition, and sent to PC after the process to reduce the time delay for the PC communication. The channel number is reduced two and PC interface changed to USB port. The signal generation of pseudo random code was installed for future improvement [17–20]. The electrical power consumption is 7W. This second-generation board is produced by Trimatiz Co., Ltd. (**Figure 9(a)**).

Other approach is tried by another company, Shibasaki Co., Ltd. [21]. PMT detector, amplifier and FPGA photon counter board was assembled in one box (**Figure 9(b)**). Single channel for a lidar echo is installed. This assembly contains a microprocessor to control the PC interface of Bluetooth. This assembly is connected to the telescope, and the lidar system does not need to wire to PC. The lidar set on the outdoor and the operator can monitor its observation inside the room. The power consumption is 2W. The LED based mini-lidar with this FPGA photon counting board could operate 2 nighttime observation (continuous 4 hours' operation per night). The minimum time resolution is 4ns, that is equivalent to the distance resolution of 0.6m. The repetition frequency follows to the LED pulse beam oscillation of 500kHz. The functional software is also bundled to visualize and analyze the observation data. The acquired data is visualized in real time.



Figure 9. Second-generation FPGA photon counter boards. Photon tracker II (Trimatiz Co., Ltd.), and (b) FPGA detection units (Shibasaki Co., Ltd.).

5. Lidar applications

The first trial of LED mini-lidar was conducted with a commercialized photon counter. SR430 produced by Stanford Research Systems was used to detect the near-range lidar echoes. It is a multi-channel scaler. The repetition frequency is 1kHz. **Figure 10** shows some of observation results. The LED mini-lidar of 100mW(=1nJ/10ns) pulse beam received atmosphere echoes in the range of 100m. The inversely proportional decay slopes indicate the atmosphere response and spike like echoes at 55m in rainy day and at 85-115m in clear day came from trees. The notable thing is its summation time. Both of the results took a time of 16 min to gather the enough signal-to-noise ratio. Long summation time is hard to detect the rapid response of the air, dust, and gas flow.

The transmitting pulse power becomes weak, its repetition frequency should be increased to have enough signal-to-noise ratio. When the pulse repetition frequency is increased 100 times,

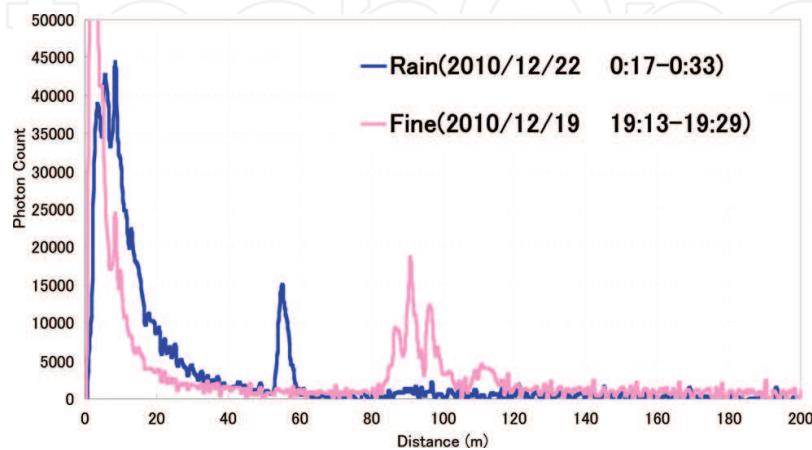


Figure 10. LED-based mini-lidar observation by commercialized photon counter (“SR430” produced by SRS).

the same signal-to-noise ratio will be obtained with the shortened time of 1/10 because of the equation (3). The LED mini-lidar increased its pulse repetition frequency till 500kHz. It is the maximum repetition frequency of the second-generation photon counting boards. In addition to this, the transmitting power also increased by changing the LED device from a Lamp-type (maximum pulse power 250mW) to a power illumination LED (maximum pulse power 1W). As a result, the summation time is shortened to 0.2s for atmosphere observation.

The first-generation photon counting board was used for atmosphere observation as shown in **Figure 11**. The LED mini lidar was improved its pulse power of 200mW ($=2\text{nJ}/10\text{s}$), the pulse repetition frequency was 380kHz. The summation time is 10s. Continuous observation of 1 hour was visualized. In this image, horizontal axis is time and vertical axis is distance. Photon counts was range corrected by multiplying the square of distance and taking log-scale, and represent with fake colors. The weather condition was clear. The atmosphere activity was low but one can see the minute change with the image. The atmosphere echoes monitored till 100 m.

When the summation time increases to 30s, the observation range increased till 300m in night time. In the daytime, the observation range was shortened till 100m under the condition that the lidar was fixed on the shade place. Even if in daytime condition, the threshold was adjusted adequately, the atmosphere activity could be monitored.

The other approach was performed by another company. Shibasaki Co., Ltd., tried to develop a high-speed photon counter and small LED lidars with their original architecture. Its structure is mentioned in section 4.3. Their LED mini-lidar transmits the pulsed beam of 250mW ($=2.5\text{nJ}/10\text{ns}$) with its repetition frequency of 400kHz. The original FPGA photon counter board has the range resolution of 0.6m, that is, 4ns with the system clock of 250MHz. The repetition frequency can follow the pulse beam oscillation of 400kHz.

Figure 12 shows the one of the observation results. It was the nighttime observation. The summation time was 30s and 50 min continuous lidar echoes was visualized as an image. The echo counts are represented by fake color with range-corrected log-scale. It was a foggy, which came from a near river. Fog activity was clearly captured and its detail can be distinguished.

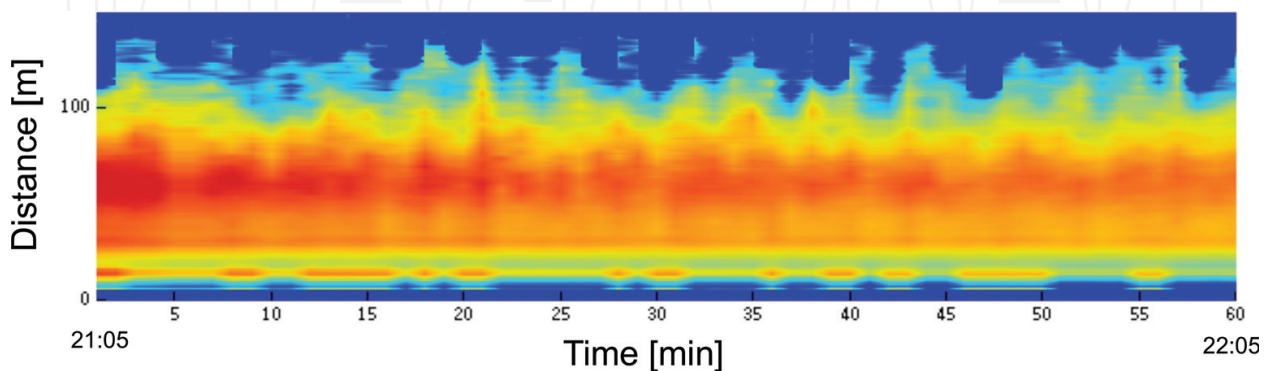


Figure 11. Atmosphere observation on August 14, 2012, by first-generation high-speed photon counter (“Photon Tracker” produced by Trimatiz Co., Ltd.).

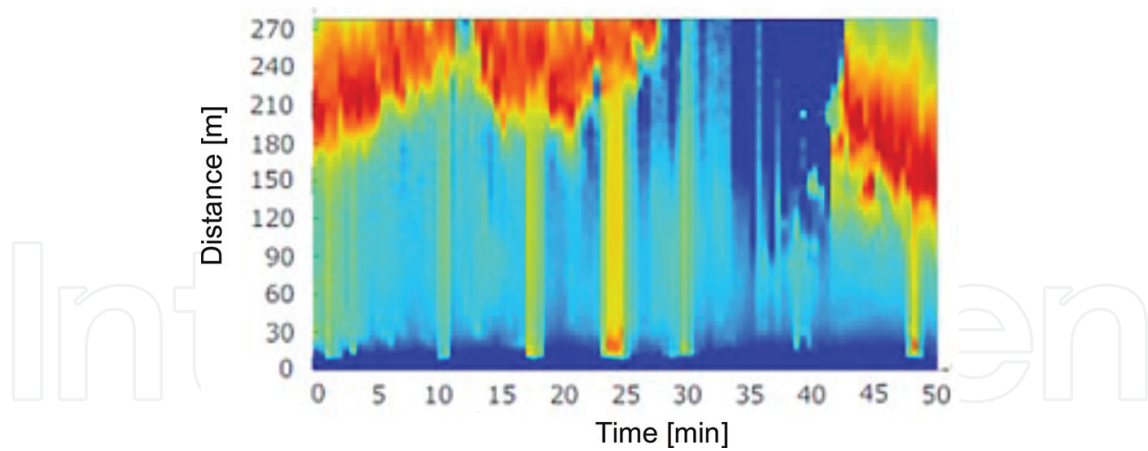


Figure 12. Fog activity observation by a LED-based mini-lidar with a new photon counter, (Shibasaki Co., Ltd.).

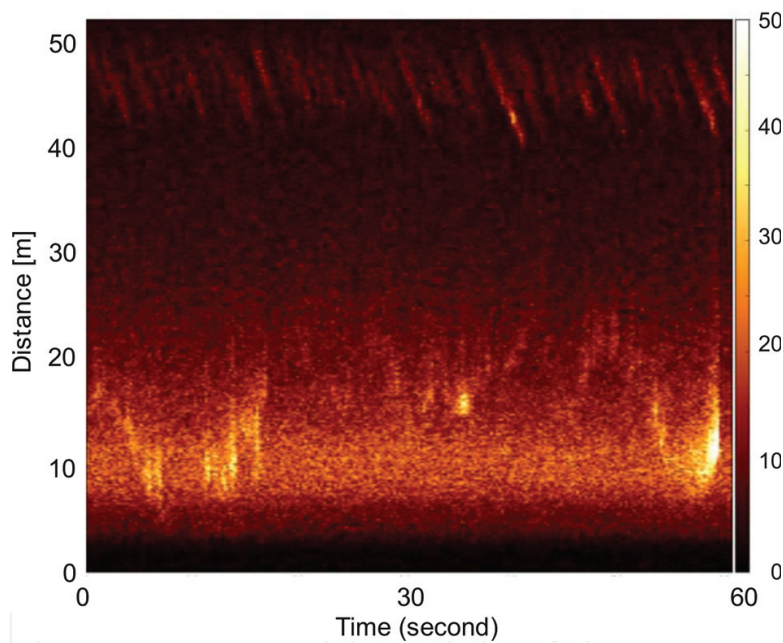


Figure 13. Sea wave observation by second-generation high-speed and high-resolution photon counter (“Photon Tracker II” produced by Trimatiz Co., Ltd.).

Suspended materials activity such as dust, fog, smoke and so on are the suitable targets for near-range lidars.

The second-generation FPGA photon counting board is adapted into the sea wave observation. The power LED beam of 0.75 W (7.5 nJ/10 ns) was installed into the lidar setup [22–24]. Its divergence is 10 mrad and the receiver’s field of view is 5 mrad. This optical setup of is the same as **Figure 3**. It was a shallow angle measurement. The LED mini-lidar was fixed on a shore and observed the sea wave washing the shore with the shallow angle of 2.5° . One of

results is shown in **Figure 13**. The summation time was 0.2 s. The range resolution was 0.15 m, that is, the BIN width was 1 ns. The wave motion is represented by fake colors, here with linear scale. It is appeared at 40–50 m. By analyzing the sea wave motion, fundamental profiles of sea wave such as wavelength, period, height and speed are deduced. The atmosphere echoes were also observed in the range of 5–40 m. The sand dusts and splashed waters were captured on the atmosphere, too. The detail of the air flow is obtained vividly. The sea wave frequency is 0.1–1 Hz. The suspended materials flow quickly on the sea surface. The short summation time and high-spatial resolution makes an identical copy of its echo activity. Dust flow on a coast, smoke motion on the chimney, whirlwind between the buildings will be visualized with this high-speed and high-resolution photon counter.

6. Summary

The near-range environmental measurement is major for safety management. In the case of car safety, the target is hard material. Its sensor is not so sensitive and becomes compact. In the near future, such sensors will be improved not only for hard target, but also suspended materials. In a tunnel accident, the smoke density, materials, gases, and their distribution, their sensing devices will give additional information for safety. In a factory, plant, and construction site, the near-range lidar will have advantage for the density measurement, distribution map, and security. Lidar is a remote sensing device, and it has an advantage against traditional contact sensors.

The low altitude atmosphere has rapid dynamics of the order to a few Hz. To follow its activity, the high-speed and high-resolution measurements are required. The traditional photon counting device cannot follow such dynamics. It is because the laser oscillation, especially high-pulse laser power is hard to follow as high repetition frequency as the a few 100 kHz.

The LED light source is one of the promising options for the lidar transmitter. Indeed, laser diode can be used with high pulse oscillation. The fiber laser increases its oscillation frequency, too. Due to this fact, light source selection is possible. With the combination of these light sources, the high-speed and high-resolution photon counting device is capable of detecting near-range atmosphere. To monitor a certain kind of gas, differential absorption method, fluorescent detection method, or Raman scattering signal detecting method will be install into the mini-lidar setup [25–30].

Author details

Tatsuo Shiina

Address all correspondence to: shiina@faculty.chiba-u.jp

Graduate School of Engineering, Chiba University, Chiba-shi, Japan

References

- [1] Bennett M, Edner H, Grönlund R, Sjöholm M, Svanberg S, Ferrara R. Joint application of Doppler Lidar and differential absorption lidar to estimate the atomic mercury flux from a chlor-alkali plant. *Atmospheric Environment*. 2006;**40**:644-673
- [2] Edner H, Ragnarson P, Wallinder E. Industrial emission control using Lidar techniques. *Environmental Science & Technology*. 1995;**29**:330-338
- [3] Noguchi Y, Miya H, Shiina T, Noguchi K, Fukuchi T, Asahi I, Sugimoto S, Shimamoto Y, Ninomiya H. Compact raman lidar for hydrogen gas leak detection. 25th International Laser Rader Conference; 2010. pp. 178-181
- [4] Raj PE, Devara PCS, Maheskumar RS, Pandithurai G, Dani KK. Lidar measurement s of aerosol col umncontent in an urban nocturnal boundary layer. *Atmospheric Research*. 1997;**45**:201-216
- [5] Gong W, Chyba TH, Temple DA. Eye-safe compact scanning LIDAR technology. *Optics and Lasers in Engineering*. 2007;**45**:898-906
- [6] Moorgawa A, Bencherif H, Michaelis MM, Porteneuve J, Malinga S. The Durban atmospheric LIDAR. *Optics and Laser Technology*. 2007;**39**:306-312
- [7] Shiina T, Ninami E, Ito M, Okamura Y. Optical circulator for an in-line-type compact lidar. *Applied Optics*. 2002;**41**:3900
- [8] Shiina T, Ninami E, Ito M, Okamura Y. In-line type micropulse lidar with an annular beam: Theoretical approach. *Applied Optics*. 2005;**44**:7467
- [9] Fujii T, Fukuchi T, editors. *Lidar Remote Sensing*. Boca Raton: CRC Press; 2005
- [10] Weitekamp C, editor. *Lidar Range-Resolved Optical Remote Sensing of the Atmosphere*. Singapore: Springer; 2005
- [11] Available from: https://www.hamamatsu.com/resources/pdf/etd/PMT_handbook_v3aE.pdf
- [12] Available from: <http://www.bgu.ac.il/~glevi/website/Guides/AvalanchePhotodiodes.pdf>
- [13] Shiina T, Koyama M. Japanese Patent Application no. 2010-275798, 2010-12-10
- [14] Koyama M, Shiina T. Light source module for LED mini-lidar. 2005;**39**(8):617-621
- [15] Grishin M, editor. Chapter 8. In: *Advances in Solid State Lasers Development and Applications*. Intech; 2010
- [16] Available from: <https://www.trimatiz.com/en/>
- [17] Takeuchi N, Sugimoto N, Baba H, Sakura K. Diode-laser random-modulation cw lidar. *Applied Optics*. 1983;**22**:1382-1386

- [18] Takeuchi N, Sugimoto N, Baba H, Sakurai K. Random modulation cw lidar. *Applied Optics*. 1986;**25**:64-67
- [19] Nagasawa C, Abo M, Yamamoto H, Uchino O. Random modulation cw lidar using new random sequence. *Applied Optics*. 1990;**29**:1466-1470
- [20] Matthey R, Mitev V. Pseudo-random noise-continuous-wave laser radar for surface and cloud measurements. *Optics and Lasers in Engineering*. 2005;**43**:557-571
- [21] Available from: <http://www.shibasaki-inc.jp/en-index.html>
- [22] Lin YC, Chang SJ, Su YK, Chang CS, Shei SC, Ke JC, Lo HM, Chen SC, Kuo CW. High power nitride based light emitting diodes with Ni/ITO p-type contact. *Solid-State Electronics*. 2003;**47**:1565-1568
- [23] Wang JC, Wang RT, Chang TL, Hwang DS. Development of 30 watt high-power LEDs vapor chamber-based plate. *International Journal of Heat and Mass Transfer*. 2010;**53**:3990-4001
- [24] Lin Y, Chen Y, Chen Z, Ma D, Zhang B, Ye T, Dai Y. Triphenylamine and quinoline-containing polyfluorene for blue light-emitting diodes. *European Polymer Journal*. 2010;**46**:997-1003
- [25] Choi S-C, Ko D-K, Lee J, Kim D-H, Cha H-K. The development of a mobile remote monitoring system by using differential absorption LIDAR technology. *Journal of the Korean Physical Society*. 2005;**49**:331-336
- [26] Devara PCS, Raj PE, Pandithurai G, Dani KK, Sonbawne SM, Rao YJ. Differential absorption lidar probing of atmospheric ozone over a tropical urban station in India. *Measurement Science and Technology*. 2007;**18**:639-644
- [27] Gondal MA, Mastromarino J. Lidar system for remote environmental studies. *Talanta*. 2000;**53**:147-154
- [28] Cecchi G, Pantani L, Raimondi V, Tomaselli L, Lamenti G, Tiano P, Chiari R. Fluorescence lidar technique for the remote sensing of stone monuments. *Journal of Cultural Heritage*. 2000;**1**:29-36
- [29] Filipčič A, Horvat M, Veberič D, Zavrtanik D, Zavrtanik M. Scanning lidar based atmospheric monitoring for fluorescence detectors of cosmic showers. *Astroparticle Physics*. 2003;**18**:501-512
- [30] Bengtsson M, Grönlund R, Sjöholm M, Abrahamsson C, Dernfalk AD, Wallström S, Larsson A, Weibring P, Karlsson S, Gubanski SM, Kröll S, Svanberg S. Fluorescence lidar imaging of fungal growth on high-voltage outdoor composite insulators. *Optics and Lasers in Engineering*. 2005;**43**:624-632

